Equilibration of a Warm Pumped Lens on a β plane

TIMOUR RADKO AND JOHN MARSHALL

Department of Earth, Atmospheric, and Planetary Sciences, Massachusetts Institute of Technology, Cambridge, Massachusetts

(Manuscript received 14 November 2001, in final form 11 October 2002)

ABSTRACT

The dynamics of a warm lens created by a surface buoyancy flux and Ekman pumping in an initially homogeneous, unbounded fluid on a β plane is studied in a set of high-resolution numerical experiments. A simple analytical model for the equilibrium structure of the lens is developed that assumes that the input of vorticity and buoyancy from the Ekman layer is balanced through transfer by baroclinic eddies that carry the warm fluid laterally away from the lens. The importance of eddy-induced diapycnal flux in the western intensification region is emphasized by developing a boundary layer theory based entirely on the cross-frontal mass exchange due to eddies. The theory is successfully tested against direct numerical eddy-resolving simulations. Possible oceanographic implications of the study for understanding subtropical gyres and the Antarctic Circumpolar Current are discussed.

1. Introduction

Homogeneous ocean circulation theory attempts to explain the broad horizontal pattern of ocean gyres by considering the absolute vorticity balance. The western boundary layer plays a central role in this balance, acting as a sink of the relative vorticity imparted to the fluid in the interior by the wind field—see, for example, the review by Stewart (1964). In thermocline theory, which focuses on the vertical structure of ocean gyres, the detailed physics of the western boundary layer has received much less attention than its homogeneous counterpart. Ideal thermocline theory ignores buoyancy and vorticity sinks and implicitly assumes that there is a *passive* nonadiabatic boundary layer that somehow balances the volume and potential vorticity budgets.

Although modern thermocline theory articulates self-consistent models that have brought much insight, one can readily question some of the underlying assumptions. Probably the most serious criticism of the ideal theories is related to our present lack of knowledge of the extent to which the ideal equations themselves are accurate in the description of the time-mean of an ocean full of energetic eddies that may have important transfer properties. Thus, the quantitative test of these thermocline theories is a test of the adequacy of the governing equations and, implicitly, the lack of importance of eddies (Vallis 2000).

Corresponding author address: Timour Radko, Dept. of Earth, Atmospheric, and Planetary Sciences, Massachusetts Institute of Technology, Rm 54-1626, 77 Massachusetts Ave., Cambridge, MA 02139.
E-mail: timour@ocean.mit.edu

In this study we consider an idealized abstraction of a subtropical ocean gyre: the equilibration of a warm pumped lens on a β plane. By construction, geostrophic eddies play a central role in the volume budget of this gyre: warm fluid pumped down from the surface is fluxed away laterally by geostrophic eddies formed as a result of the baroclinic instability of a large-scale current. In a recent paper (briefly reviewed in section 2), Marshall et al. (2002) described these processes in an f-plane framework. Here we extend this work to the β plane. A fundamental difference between the Marshall et al. (2002) study and the present one is that now, because of β, eddy shedding (as well as the intensity of the mean flow) is not distributed uniformly around the lens but is strongly enhanced on the western flank of the lens.

We show in a series of numerical experiments, in which the value of β is varied while keeping other parameters fixed, that, in the limit of strong β, eddy processes are confined to a thin ''boundary'' layer at the western edge of the lens. The resulting time-mean states in the large β case prove to be very suggestive of the structure and dynamics of ocean gyres. The equilibrated lens can be described as a quasi-adiabatic Sverdrupian gyre bounded on the west by a narrow eddying intensification region. The nature of this western boundary layer is studied and its role in closing the circulation is explored. In the opposite limit when β is small, the eddies dominate the whole solution and Sverdrup dynamics cease to be a constraint. In this case we find that the dynamics of the lens become analogous to that of a circumpolar jet (Karsten et al. 2002), in which the tendency of mechanical and thermodynamic forcing to

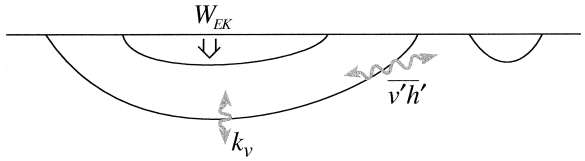

FIG. 1. Schematic representation of a pumped heated lens. An important question is whether the equilibration of the lens is accomplished by the lateral eddy flux $\overline{v'h'}$ or by the vertical mixing k_v.

tilt isopycnals is balanced by eddies, which tend to flatten them. The eddies are very effective in exchanging fluid across the front and play a central role in setting its stratification and vertical structure.

The numerical results are interpreted in terms of a simple analytical model based on a parameterization of eddy fluxes in which the intensity of the cross-layer mass flux is assumed to be a function of the mean flow. We are able to capture in one theoretical framework the dynamics relevant to Sverdrupian gyres as well as circumpolar jets, depending on the relative values of β and a parameter representing the intensity of eddy shedding.

2. Equilibration of warm, pumped lenses

Consider a subtropical ocean forced by anticyclonic wind stress; Ekman layers pump the warm fluid down into the interior, generating vertical stratification, as sketched schematically in Fig. 1. In the steady state the continuous flux of buoyancy into the main thermocline must be balanced by an equivalent buoyancy sink. One view [first expressed by Robinson and Stommel (1959) and studied more recently by, e.g., Samelson and Vallis (1997)] assumes that small-scale mixing, characterized by k_v, plays a central role in achieving such a balance. An alternative possibility, explored by Marshall et al. (2002), is that the warm fluid pumped down from the surface is continuously fluxed away laterally by geostrophic eddies, as indicated in the schematic diagram, Fig. 1. Here we explore the dynamical consequences of this idea by abstracting the problem to that of a warm pumped lens on a β plane.

a. f plane

It is useful to consider the limit case in which transfer by geostrophic eddies—a process that is completely absent from ideal thermocline theory—is the controlling factor in setting stratification. Marshall et al. (2002) studied the temperature anomaly and depth of penetration of a warm lens created by a surface buoyancy flux and Ekman pumping in an initially homogeneous, rotating fluid on an f plane. In a set of laboratory and numerical experiments, Marshall et al. demonstrated that the deepening of the warm lens is arrested by eddies that form as a result of a baroclinic instability of the density front and sweep fluid laterally away from the heated lens.

Analytical theory developed by Marshall et al. to describe this phenomenon was based on a simple parameterization of eddy transfer in which the transfer coefficients depended on the strength of a density front. Of course, such a theory implicitly assumes that the rate of irreversible mixing (eventually accomplished by molecular effects acting on the microscale) is controlled by geostrophic eddies. It is not yet clear to what extent this is realized in the ocean. Nevertheless, this theory yields a simple prediction for the depth scale of the lens h_{dim}, which was confirmed by laboratory and numerical experiments:

$$h_{\text{dim}} = c_h \left(\frac{f_{\text{dim}}}{B} \right)^{1/2} W_e L; \qquad B = W_e g', \tag{1}$$

where B is a scale of the surface buoyancy flux, W_e is a scale of the Ekman pumping, g' is the reduced gravity, L is the lens diameter, and f_{dim} is the Coriolis parameter. The nondimensional constant c_h characterizes the efficiency of eddy buoyancy transfer (to be discussed below). Now we extend this model to a more oceanographically relevant problem—the warm, pumped lens on a β plane.

b. β plane

An obvious limitation of the f-plane lens studied in Marshall et al. (2002), which makes its relevance to ocean gyres uncertain, is that there is no gradient in planetary vorticity. One of the features that distinguish the β-plane and f-plane models is that in the former case it is possible to construct meaningful theories for the thermocline depth that are based on purely adiabatic considerations (e.g., Luyten et al. 1983). The depth scale that appears in such models is given by

$$h_{\text{dim}} = \sqrt{\frac{2LW_e f_{\text{dim}}^2}{g'\beta}}, \tag{2}$$

as can be shown by applying the Sverdrup relation to the upper active ocean layer (e.g., Pedlosky 1996).

To determine the relative merits of the models based on (i) eddy-transfer and (ii) ideal theories in the description of an eddying gyre, we now create a warm pumped lens on a β plane and study its evolution numerically. The numerical setup represents a lens in an ''unbounded'' ocean, so that the eddies are able to propagate over large distances away from the lens, effectively acting as sinks of buoyancy and vorticity. Such a model makes it possible to isolate the physical processes of interest and to unambiguously interpret the fundamental dynamics at play.

1) NUMERICAL SETUP

We solve the Boussinesq form of the incompressible Navier–Stokes equations in a rotating frame using the numerical model described in Marshall et al. (1997a,b).

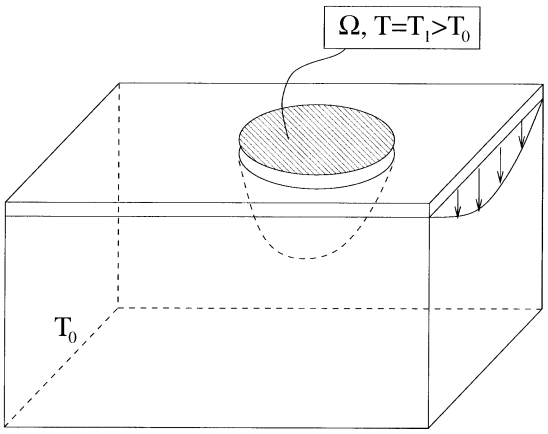

FIG. 2. Schematic representation of the numerical experiment. At the upper surface, the fluid is forced by zonal winds, corresponding to the Ekman pumping vanishing at the meridional boundaries. Fluid is pumped down within a circular region Ω (shaded area) at temperature T_1 into initially resting fluid of (colder) temperature T_0. An asymmetric (due to β) warm lens forms directly below the heating zone Ω.

Computations are made in a rectangular box on whose walls normal flow is set to zero. There are 248 $\times$ 124 $\times$ 30 grid elements. The flow is set in motion by applying a zonal wind stress which corresponds to the Ekman pumping velocity vanishing at the northern and southern boundaries of the basin ($-L/2 < y < L/2$):

$$w_e = -W_e \cos(\pi y/L). \tag{3}$$

Fluid is also thermally forced by locally warming the surface layers within a (smaller) circular region (Ω), as shown in a schematic in Fig. 2. As mentioned above, to avoid consideration of the possibly complex interaction of our warm lens with rigid boundaries, the heating zone Ω is placed in the eastern part of the basin. Technically, an input of buoyancy is accomplished by relaxing the Ekman layer temperature in the region Ω to a value T_1 exceeding the nominal ambient temperature of the fluid T_0 by $\Delta T = 10$°C.

The depth of the basin is chosen so as to result in a flow with no significant near-bottom velocities below the lens, and the vertical structure of the flow is resolved using a nonuniform mesh with the grid spacing decreasing upward. The horizontal grid spacing is sufficient to resolve the first baroclinic radius of deformation (by at least three grid points) in all the numerical experiments described. In order to maintain a connection with the corresponding f-plane experiments in Marshall et al. (2002) and Karsten et al. (2002), their numerical setup was modified only as little as possible (with varying Coriolis parameter being the main change). The reader interested in numerical details is referred to those papers for a more complete description of the numerics.

2) EVOLUTION OF THE LENS

The model was initialized from rest with water of uniform temperature, and, after a few rotation periods, a quasi-steady mechanically driven barotropic circulation was established. Figure 3 shows the subsequent formation and evolution of a buoyant lens directly below the heating zone Ω for the case of a moderate beta effect. At first (see Fig. 3a), the lens uniformly deepens as the light fluid is pumped down from the Ekman layer, and starts to rotate anticyclonically in accord with thermal wind balance. The next stage of the flow evolution (Fig. 3b) is characterized by further deepening and accelerated rotation of the lens. At the same time the lens starts to ''feel'' the β effect and shifts westward. This asymmetry, already apparent in Fig. 3b, results in a thermal wind shear that is much higher on the western side of the lens than it is on the eastern side.

Because the deformation radius set up in the lens is considerably smaller than its scale, the flow eventually becomes baroclinically unstable, as discussed in Marshall et al. (2002). However, in contrast to f-plane experiments, this instability is not distributed uniformly around the lens but is localized in the region of strong thermal wind velocities. The instability manifests itself in the formation of irregular eddies on the left (westward) side of the lens in Fig. 3c. These eddies grow, detach, and then move away from the lens. Figure 3d shows the already mature, equilibrated lens which disposes of the influx of buoyancy from the Ekman layer by continuous eddy shedding.

Inspection of the velocity vectors, superimposed on the horizontal temperature cross section in Fig. 4, reveals the extreme disorder and chaotic nature of the eddy shedding. The flow field to the left of the lens includes several pronounced coherent vortices that move westward under the combined influence of the β effect and advection by weak barotropic flow. These vortices are surrounded by much more irregular and short-lived structures. A different signature of baroclinic instability appears on the eastern flank of the lens, where eddies appear in the form of nonlinear wavelike perturbations (see Fig. 4). The latter, however, generally do not evolve into isolated vortices and remain attached to the lens, apparently playing only a minor role in the volume balance of the lens.

3) TIME-MEAN FIELDS

Among the various characteristics of the geometrical shape of the lens, it is its east–west symmetry that seems to be affected most by inclusion of, and variations in, β. Even a brief look at the perfectly symmetric f-plane lenses in Marshall's experiments and the present tilted solutions gives an idea of how dramatic are the changes caused by inclusion of the β effect. Asymmetry is clearly visible even when the β effect is relatively weak (as is the case for the flow in Fig. 5).

To analyze systematically how the equilibrium shape of the lens changes as a function of β, we now perform a set of experiments in which β is varied while other parameters are kept constant. In Fig. 6 we superimpose

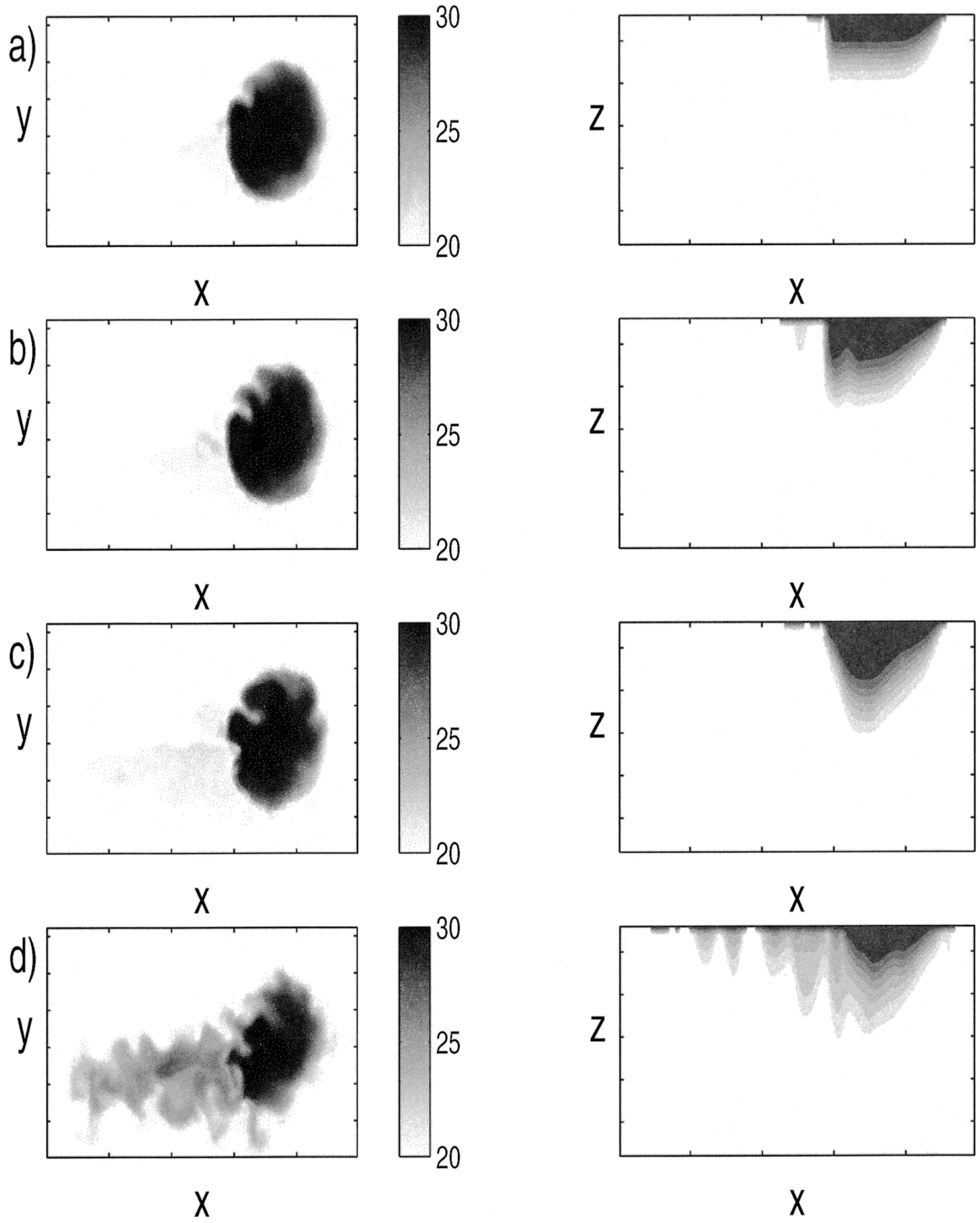

FIG. 3. Evolution of the numerical lens: (left) a horizontal cross section of the temperature field just below the Ekman layer, after 10 000/(2π), 20 000/(2π), 40 000/(2π), and 60 000/(2π) periods of rotation; (right) corresponding east–west vertical (x–z) temperature sections.

the zonal sections of the time-mean $T_2 = 0.5(T_1 + T_0)$ isotherms from each run. As is apparent from Fig. 6, the lens responds to the increase in β by becoming more and more asymmetric. For large values of β, the western side of the lens (to the left of the depth maximum) reduces to a thin boundary layer while the eastern part is apparently governed by adiabatic Sverdrup dynamics.

What is the basic physics involved in the equilibration of the lens in general and in the maintenance of the internal boundary layer (Fig. 6) in particular? The flow

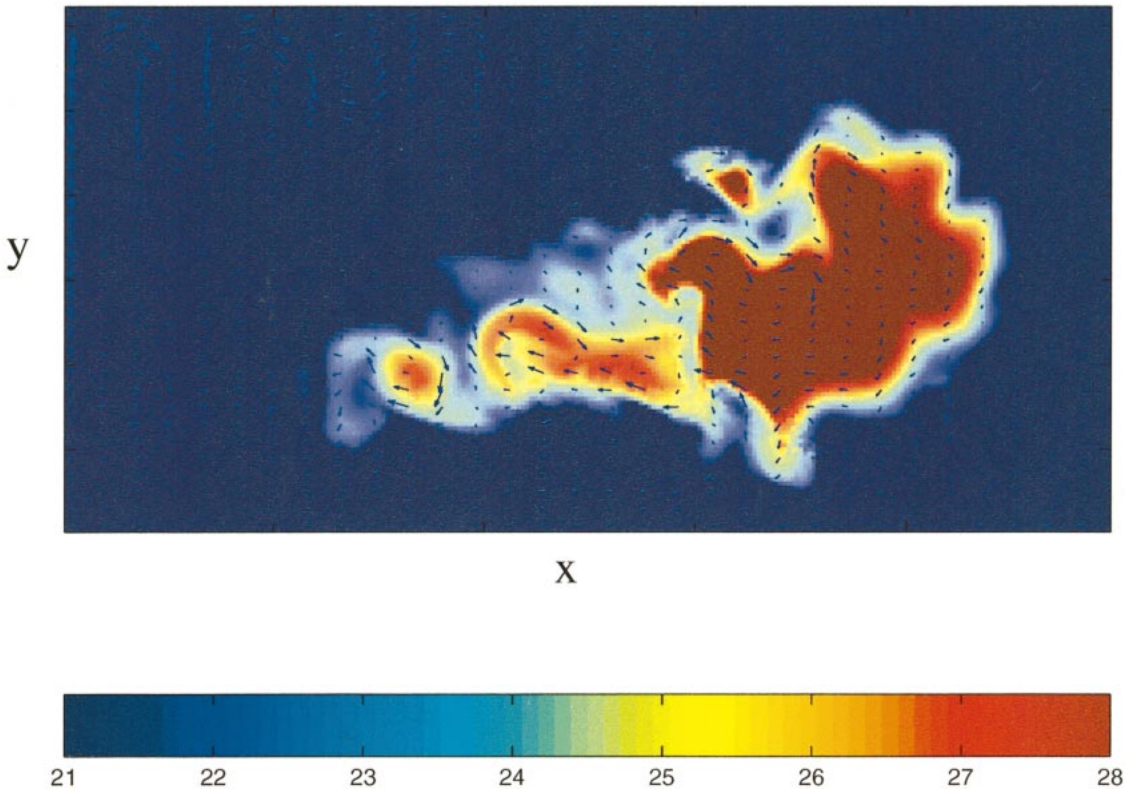

FIG. 4. Snapshot of the flow field, horizontal cross section. Horizontal velocities (arrows) are superimposed on the temperature field.

patterns shown in Figs. 3 and 4 provide some clues as to the dynamics of equilibration. We observe that the influx of warm water from the Ekman layer in a β-plane lens is balanced by the volume loss due to eddy shedding and that the eddy activity greatly increases in a region of strong mean currents. Guided by these observations, we now develop a simple theory that is based on flow-dependent cross–isopycnal eddy transfer. This model will be used to interpret the structure of the mean fields and their dependence on β.

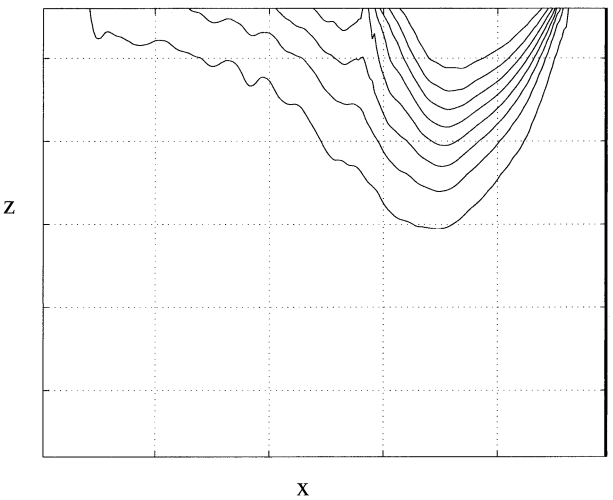

FIG. 5. Vertical (x–z) cross section of the numerical time-mean temperature field for the run in Figs. 3 and 4. Means are averaged over 50 data files recorded in the time interval $20\,000 < t < 120\,000$. The decaying ''tail'' in the western part of the basin is a contribution from the eddies continuously shed by the lens.

3. Theoretical model of equilibrated lenses

Our starting point is a 1½-layer shallow-water fluid with a mass source representing Ekman pumping and a mass sink due to eddy-shedding processes. We suppose that the depth of the lens vanishes at its (circular) periphery. The flow is assumed to be in hydrostatic and geostrophic balance, and the Coriolis parameter varies linearly in y. The system of nondimensionalization is based on the lateral scale of pumping L, the value of the Coriolis parameter at the basin center f_0, and the (positive) maximum amplitude of the Ekman pumping W_e, used as a scale for the vertical velocity. The corresponding scales of the horizontal velocity U, vertical scale H, and planetary vorticity gradient β are

$$U = \sqrt{\frac{g' W_e}{f_0}}; \qquad H = \sqrt{\frac{f_0 W_e}{g'}} L; \qquad \beta = \frac{\beta_{\text{dim}} L}{f_0}. \quad (4)$$

Under these assumptions, the governing shallow-water equations are, in the time mean,

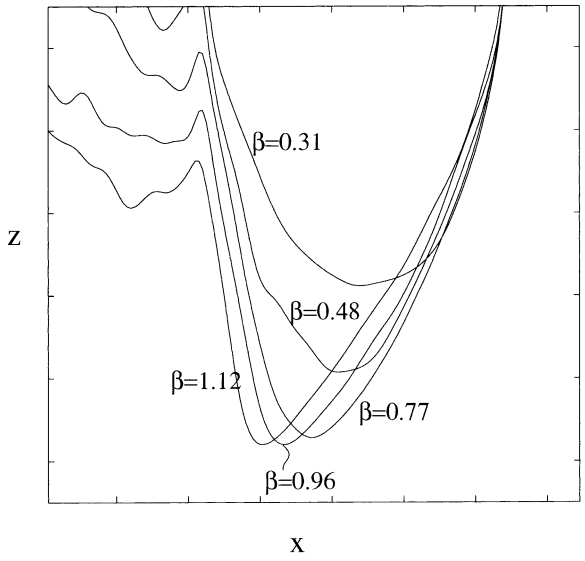

FIG. 6. Zonal cross sections of the time-mean T_2 isotherms from various experiments are superimposed to demonstrate formation of a thin western boundary layer as β increases. Nondimensional units are used in which $\beta = (\beta_{\text{dim}}L)/f_0$, where L is the lens diameter and f_0 is the Coriolis parameter at the center of the lens.

$$(1 + \beta y)u = -\partial h/\partial y$$
$$(1 + \beta y)v = \partial h/\partial x$$
$$\frac{\partial}{\partial x}(uh) + \frac{\partial}{\partial y}(vh) + w_e + w^* = 0, \tag{5}$$

where h is the nondimensional thickness of the upper layer and (u, v) is the horizontal velocity, w_e is the Ekman velocity (negative for pumping), and the cross-isopycnal volume flux is represented by w^*, where

$$w^* = \nabla \cdot (\overline{\mathbf{v}'h'}). \tag{6}$$

We assume that this ''bolus flux'' is dominated by the contribution from geostrophic eddies that move laterally away from the lens and thereby continuously transport light fluid across the isopycnals.

To simplify the system (5), just as in deriving the Sverdrup relation, we multiply the geostrophic equations [(5)] by h and then add the y derivative of the first (u) equation to the x derivative of the second (v) equation. We then eliminate the horizontal flux convergence in the volume equation to arrive at (in nondimensional units):

$$\frac{\beta}{f}\frac{\partial h}{\partial x}h = f(w_e + w^*), \tag{7}$$

where $f = 1 + \beta y$, $(-\frac{1}{2} < y < \frac{1}{2})$, and the Ekman pumping is $w_e = -\cos(\pi y)$, as in the foregoing numerical experiments.

It is intuitively clear that the local behavior of the sought after solutions of (5) will be determined by the value of w^* relative to w_e. In the flow regions where w^* is small, the dynamics are expected to be essentially Sverdrupian, whereas if w^* is large the flow is controlled the eddy-related processes. Below we will elaborate this simple idea. First it is necessary to close the problem (5) and to explicitly specify how (and whether) the mass flux w^* depends on the local properties of the large-scale flow.

A number of ideas about how to parameterize the isopycnal and diapycnal transports by eddies have been suggested in the literature, as reviewed, for example, in Visbeck et al. (1997). We will focus on one of the simplest closures for (6) corresponding to thickness diffusion $w^*_{\text{dim}} = -K_{\text{dim}}\nabla^2 h_{\text{dim}}$, because it is generally consistent with the qualitative properties of eddies observed in our numerical experiments (see section 4). One can question the specific form of the eddy closure assumed, and so we describe and analyze an alternative parameterization in an appendix. Differences and similarities between the two models can be used to separate the relatively robust features of the resulting solutions from the closure-dependent ones.

a. Thickness-diffusion closure: $w^* \propto \nabla^2 h$

The ''thickness-diffusion'' closure is a relatively common parameterization, which appears, for example, in the Gent and McWilliams (1990) model. In nondimensional variables it reduces to

$$w^* = -C\nabla^2 h, \tag{8}$$

where

$$C = \frac{K_{\text{dim}}}{LU}, \tag{9}$$

and the governing equation (7) becomes

$$\frac{\beta}{f}\frac{\partial h}{\partial x}h = -f[\cos(\pi y) + C\nabla^2 h]. \tag{10}$$

Note that (10) is mathematically analogous to the expression that appears in the Stommel (1948) problem but with nonlinearity retained in the dispersive term. Apart from the diffusive term, (10) is similar to the expression for the upper-layer equation of ventilated thermocline models. However, it is important to emphasize that the physical mechanism of equilibration in our model is completely different, as is the interpretation of the diffusive term. The term represents the eddy bolus transport, (6), as sketched in Fig. 1.

The ''modified Sverdrup equation'' [(10)] now has to be solved subject to the boundary condition $h = 0$ along the lens boundary [$r = \sqrt{(x - 0.5)^2 + y^2} = 0.5$]. Before presenting some explicit asymptotic solutions (section 3b), we first consider the typical numerical results. Integration of (5) (with added time derivatives) using a simple finite-difference code yields the steady lens solution presented in Fig. 7. Parameters chosen were $\beta = 0.5$ and $C = 0.01$, which roughly represent the situation in ocean gyres.

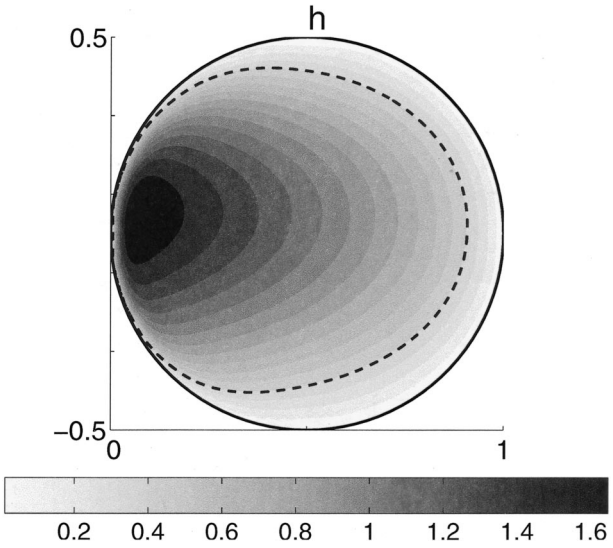

FIG. 7. Upper-layer depth for the steady state obtained by the numerical integration of (5) for $\beta = 0.5$ and $C = 0.01$. Dashed line represents the trajectory of a Lagrangian particle ($h = \text{const} = 0.4$).

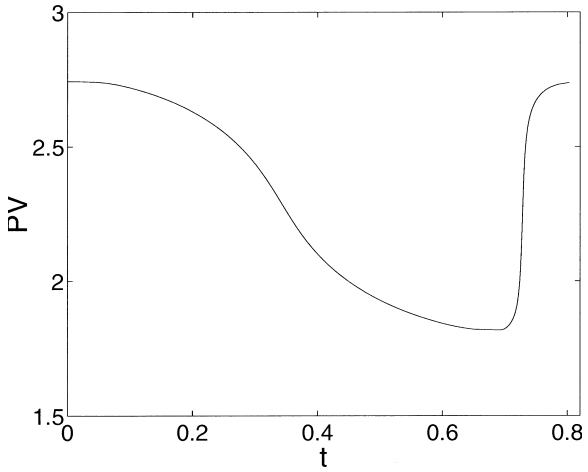

FIG. 8. Variation of the potential vorticity following the Lagrangian particle moving clockwise along the trajectory shown in Fig. 7. Note the rapid increase of PV as the particle passes through the boundary layer.

The most prominent feature of the lens shown in Fig. 7 is a thin western intensification zone connected to a ''Sverdrup'' interior. The boundary layer in Fig. 7 is entirely due to eddy buoyancy transfer and is unrelated to lateral and/or bottom friction. The dynamics of equilibration can be understood by considering the vorticity and buoyancy budgets of the lens.

Fluid pumped down from the Ekman layer is uniformly light ($\rho \equiv \rho_1$) relative to the abyssal water ($\rho = \rho_2 > \rho_1$). Thus, there is a constant flux of buoyancy into the lens, and a steady state can only be achieved through the detrainment of warm water by eddies (w^*). This can be confirmed by integrating the third equation in (5) over the area of the lens, which yields, in the steady state,

$$\iint w_e \, dS = -\iint w^* \, dS. \tag{11}$$

In the eastern part of the lens (see Fig. 7), the nondimensional scale for the cross-layer flow [see (10)] yields $w^* \sim C \ll 1$ if $\beta = O(1)$: w^* over the interior only makes a minor contribution to the integral in (11). On the other hand, the spatial gradients in the western intensification zone are large, as are the values of w^*, thus making it possible to satisfy the global flux integral (11).

Processes in the western boundary layer are also essential for closing the vorticity budget. Derivation of the shallow-water potential vorticity equation for our system (5) yields

$$\frac{D}{Dt}\text{PV} = \text{PV}\left(\frac{w_e + w^*}{h}\right), \tag{12}$$

where potential vorticity $\text{PV} = f/h$. Because every streamline is closed, it follows from (12) that, as the upper-layer column makes a full circle around the basin, the decrease of PV due to Ekman pumping (negative w_e) is exactly compensated by the volume release by eddies (positive w^*). Figure 8 shows the variation in time of the potential vorticity for a Lagrangian column as it moves along the trajectory marked in Fig. 7 (moving clockwise from the most northern point on the streamline). This figure gives an indication of the spatial distribution of the sources and sinks of PV. The net loss of PV during the time the particle spends in the gyre interior [$0 < t < 0.68$, where t is a nondimensional time based on U and L; (4)] is rapidly compensated by the PV gain as it passes through the boundary layer ($0.68 < t < 0.8$), where the local spatial scales are small and therefore $w^* \sim \nabla^2 h$ is large.

Inspection of the flow pattern in Fig. 7 helps us to identify distinct dynamical regimes in (C, β) parameter space. In the quasi-Sverdrupian interior the lhs of (10) is balanced by Ekman pumping, the first term on the rhs. Thus, with $\partial/\partial x$, $f \sim 1$,

$$h \sim \beta^{-1/2}. \tag{13}$$

The corresponding interior nondimensional cross-layer flux [(8)] is

$$w^* \sim Ch \sim \frac{C}{\sqrt{\beta}} = \epsilon, \tag{14}$$

where

$$\epsilon = \frac{C}{\sqrt{\beta}} = \frac{K_{\text{dim}}}{LU}\sqrt{\frac{f_0}{\beta_{\text{dim}} L}}. \tag{15}$$

We now go on to show that ϵ controls several important characteristics of the solution. Noting that $K_{\text{dim}} \sim (w^* L^2)/h_{\text{dim}}$ and using (4) for the scale of h_{dim}, we can write (15) as

$$\epsilon \sim \frac{w^*_{\rm dim} L}{\sqrt{\dfrac{2 f_0^2 W_e L}{g' \beta_{\rm dim}}} \sqrt{\dfrac{g' W_e}{f_0}} \sqrt{\dfrac{f_0}{\beta_{\rm dim} L}}} \sim \frac{w^*_{\rm dim}}{W_e}, \qquad (16)$$

where W_e is a scale for the dimensional Ekman pumping and $w^*_{\rm dim}$ is the dimensional diapycnal volume flux due to eddies. Thus ϵ can be thought of as a measure of importance of the diapycnal eddy transfer relative to the vertical advection in the interior of the lens. In particular, the interior is quasi-adiabatic as long as $\epsilon \ll 1$.

b. Analytical formulation

To illuminate the underlying physics further, we now present some explicit analytical solutions by exploring the important asymptotic limit $\epsilon \ll 1$. As argued above, this limit corresponds to a regime in which the eddy processes are weak relative to the β effect over most of the lens area, a situation which we expect to be realized in the ocean. First, we rewrite the equations of motion (10) in polar coordinates:

$$\frac{\beta}{f^2} h \left[\frac{\partial h}{\partial r} \cos(\theta) - \frac{1}{r} \frac{\partial h}{\partial \theta} \sin(\theta) \right] + \cos(\pi y) + C \left(\frac{\partial^2 h}{\partial r^2} + \frac{1}{r} \frac{\partial h}{\partial r} + \frac{1}{r^2} \frac{\partial^2 h}{\partial \theta^2} \right) = 0, \qquad (17)$$

where $r = \sqrt{(x - 0.5)^2 + y^2}$, $\sin(\theta) = y/r$, $\cos(\theta) = (x - 0.5)/r$, and the boundary condition is $h = 0$ at $r = 1/2$. As in Stommel's theory modified for a circular basin by Pedlosky and Greenspan (1967), we separately consider the ideal interior region and a thin western boundary at $(1 - r) < \epsilon$, $\cos(\theta) < 0$. The interior solution is obtained by setting $C = 0$ in (17) and integrating the result zonally:

$$h_I^2 = \frac{2 f^2}{\beta} \left(-x + \sqrt{\frac{1}{4} - y^2} \right) \cos(\pi y). \qquad (18)$$

The boundary layer equation is obtained by stretching the radial coordinate near the lens boundary as $(\tfrac{1}{2} - r) = \epsilon \xi$ and taking the $\epsilon \to 0$ limit. The result can be written in terms of ξ as

$$-\sqrt{\beta} h_B \frac{\partial h_B}{\partial \xi} \cos\theta + f^2 \frac{\partial^2 h_B}{\partial \xi^2} = 0. \qquad (19)$$

The expression in (19) depends on θ parametrically and therefore can be directly integrated in ξ. Integrating it once in ξ results in

$$\sqrt{\beta} \frac{h_{I0}^2 - h_B^2}{2} \cos\theta + f^2 \frac{\partial h_B}{\partial \xi} = 0, \qquad (20)$$

where

$$h_{I0}(\theta) = h_I(r, \theta) \quad \text{at } r = 1/2, \qquad \cos\theta < 0 \qquad (21)$$

is the interior solution (18) immediately outside of the boundary layer. Note that in (20) we have already used the matching condition $\lim_{\xi \to \infty} h_B = h_{I0}$. A second integration in ξ yields

$$h_B = h_{I0} \tanh \left[-\frac{\xi \cos(\theta) \sqrt{\beta} h_{I0}}{2 f^2} \right], \qquad (22)$$

where we have taken advantage of the boundary condition $h_B = 0$ at $\xi = 0$.

The dependence of a characteristic boundary layer width δ on the governing parameters can be deduced by considering a fixed phase of the expression in (22):

$$-\frac{\xi \sqrt{\beta} h_{I0} \cos\theta}{2 f^2} = \text{const} = O(1). \qquad (23)$$

When this expression is evaluated along the zonal section across the lens center ($y = 0$) where $f = 1$, $\theta = -\pi$, we obtain, returning to the original nondimensional units of length $\delta = \epsilon \xi$,

$$\delta \propto C/\sqrt{\beta} = \epsilon, \qquad (24)$$

where h_{I0} is eliminated using (18).

To be specific, let us define δ as the width of the northward return flow estimated from the deepest point at the zonal section across the lens center. For the numerical solution in Fig. 7, $\delta = 0.07$ and $\epsilon = 0.014$. Thus the numerical factor in (24) is 5 and

$$\delta = 5\epsilon. \qquad (25)$$

Equation (25) indicates how the structure of the boundary layer depends on the governing parameters of the problem. As anticipated earlier, the scale for its width is set by ϵ. The boundary layer narrows when β is increased (for a fixed C) or C is decreased (for a fixed β).

The explicit solution given by (18) confirms that in the $\epsilon \to 0$ limit the total volume of the upper layer fluid, as well as the depth of the thermocline, can be understood without invoking eddies. On the other hand, the eddy buoyancy transfer is fundamental in the vicinity of the western boundary current, where the intense eddy shedding balances the total influx of buoyancy from the Ekman layer and determines the structure of the intensification region. Of course, the situation is very different in the opposite limit when ϵ is large (f-plane approximation). From the structure of the governing equation (17) it is clear that for $\beta = 0$ the flow pattern has to be zonally symmetric and the eddy shedding significant throughout the lens area. This was the limit studied in Marshall et al. (2002).

4. Comparison of the theory and numerical eddy-resolving simulations

We now present additional diagnostics of the numerical solution that support the foregoing theoretical model. Because the theory is based on the parameterization of the cross-layer fluxes, it becomes crucial to

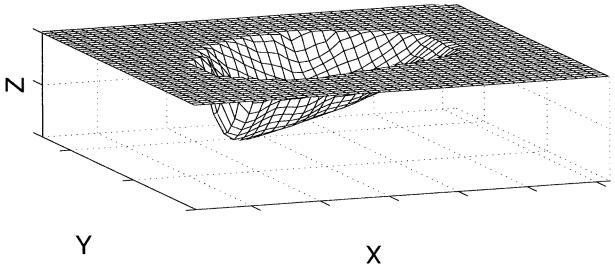

FIG. 9. Spatial structure of the time mean isotherm $T = T_0 + 7°$ for $\beta = 1.12$. Note the pronounced meridional asymmetry of the lens.

demonstrate that they are correlated with the strength of the mean current. Consider the experiment in Fig. 6 corresponding to the largest value of β employed ($\beta = 1.12$). Figure 9 shows one of the mean isopycnals ($T = T_0 + 7°$) that outcrop within the area of heat input (Ω) in that experiment. Although comparison of the continuously stratified and reduced-gravity models is not exact, as a first step it is sensible to use the depth of one of the isotherms (e.g., Fig. 9) in the stratified model as a counterpart of the active layer thickness in our theory. Likewise, the upper-layer volume loss term (w^*) in the theory directly corresponds to the diapycnal buoyancy transfer in the stratified model:

$$w^* = \overline{w} - \left[\overline{u}\frac{\partial}{\partial x}z(\overline{T}) + \overline{v}\frac{\partial}{\partial y}z(\overline{T})\right], \qquad (26)$$

where $z(\overline{T})$ is the depth of an isopycnal surface. When the slope of isopycnals is expressed in terms of the buoyancy gradients as

$$\frac{\partial}{\partial x}z(\overline{T}) = -\frac{\overline{T}_x}{\overline{T}_z} \quad \text{and} \quad \frac{\partial}{\partial y}z(\overline{T}) = -\frac{\overline{T}_y}{\overline{T}_z}, \qquad (27)$$

(26) reduces to

$$\overline{u}\overline{T}_x + \overline{v}\overline{T}_y + \overline{w}\overline{T}_z = w^*\overline{T}_z. \qquad (28)$$

The divergence of the time-mean buoyancy fluxes on the lhs of (28) is equal, in the steady state, to the sum of the eddy transfer term $-\nabla(\overline{\mathbf{v}'T'})$ and effects of small-scale diffusion. We can therefore readily isolate the eddy-driven component of w^*:

$$w^*_{\text{eddy}} = -\frac{\nabla \cdot (\overline{\mathbf{v}'T'})}{\partial\overline{T}/\partial z}. \qquad (29)$$

We now diagnose (29) directly from eddy fluxes diagnosed from the numerical simulations—plotted in Fig. 10a—and compare it with (8) using the depth of the isotherm in Fig. 9 for h. The spatial patterns of w^*_{eddy} (Fig. 10a) and $\nabla^2 h$ (Fig. 10b) turn out to be remarkably similar, with strong intensification near the western edge of the lens. Such a strong correlation between w^* and $\nabla^2 h$ is significant for a number of reasons. In addition to lending support to the closure, (8), it allows us to estimate the constant C directly. Ratio of the rms amplitudes of w^* and $\nabla^2 h$ in Fig. 10 implies the eddy

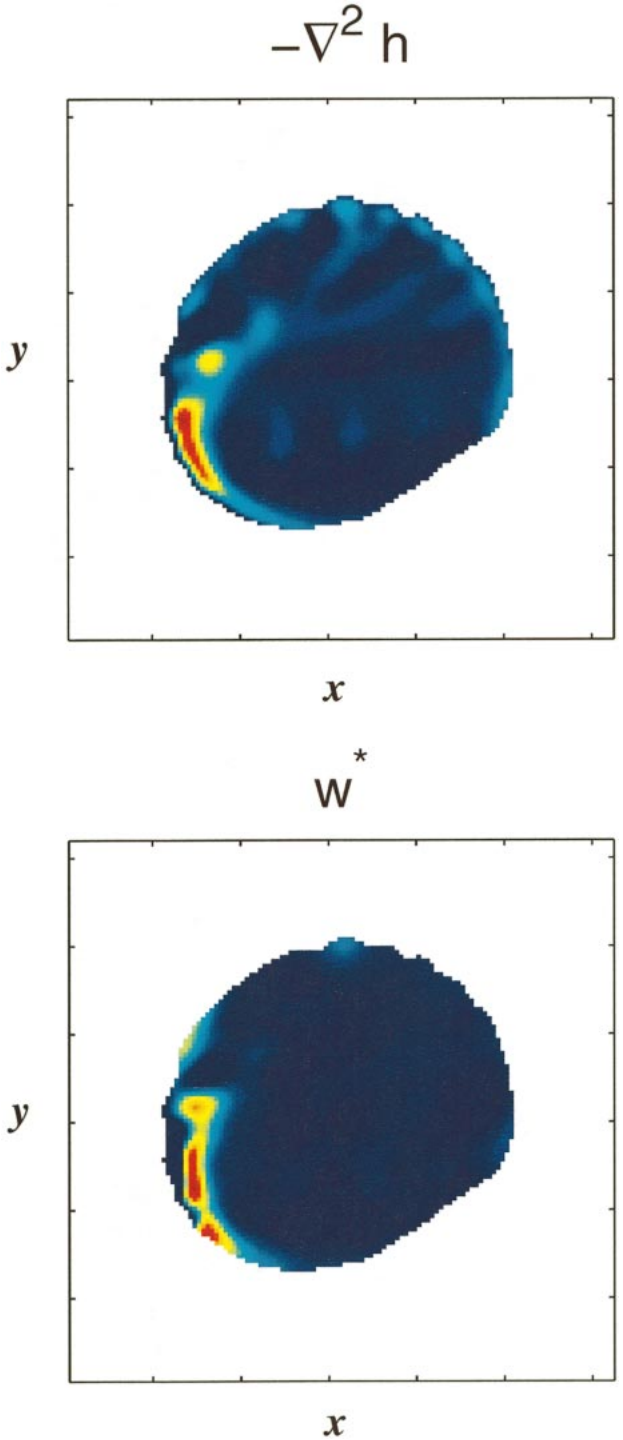

FIG. 10. Diagnostics of the numerical experiment for the strong β regime: (a) strength of the mean flow as measured by $\nabla^2 h$, where h is the depth of the isopycnal shown in Fig. 9; (b) intensity of the cross-isopycnal eddy transfer (w^*). Note the apparent spatial correlation between the two.

transfer constant is about $C = 0.04$, close to that found in, for example, Jones and Marshall (1997), in a different context.

Direct diagnostics of the eddy-induced cross-isopycnal flux also makes it possible to quantify the relative significance of the eddy transfer and numerical diffusion in equilibrating the lens. Pumping of the incompressible fluid from the Ekman layer into the volume bounded by the outcropping isopycnal (e.g., Fig. 9) has to be balanced, in a steady state, by the flux across this isopycnal. Because the total diapycnal volume flux includes both the eddy transfer (w^*_{eddy}) and a contribution from the numerical diffusion, a meaningful measure for the role of eddies is given by a parameter

$$\alpha = \frac{\iint w^*_{\text{eddy}}\, dx\, dy}{\iint w_e\, dx\, dy}, \tag{30}$$

where the integration of w_e is carried out over the area bounded by the outcrop curve, and the w^* in the numerator of (30) is evaluated at the corresponding isopycnal surface. The expression in (30) has been computed for the isotherm in Fig. 9, resulting in the eddy contribution parameter $\alpha = 0.81$. This value implies that explicit diffusion in our experiment accounts for only a fraction ($\sim$19% at most) of the cross-isopycnal volume flux. Analogous diagnostics (not shown) have also been made for the potential vorticity, and the results confirmed that the global PV budget is, at the leading order, represented by a balance between the effects of Ekman pumping and eddy buoyancy transfer as implied in (12).

It should be mentioned that the values of vertical diffusivity in our numerical experiments are realistic. The nondimensional vertical diffusivity employed is $1/P_e = k_v/(W_e H) = 0.1$. On oceanic scales ($L \sim 2 \times 10^6$ m, $f_{\text{dim}} \sim 10^{-4}\ \text{s}^{-1}$, $W_e \sim 10^{-6}\ \text{m s}^{-1}$, $g' \sim 0.01$), our diffusivity is equivalent to $k_v \sim 2 \times 10^{-5}\ \text{m}^2\ \text{s}^{-1}$, which is comparable to the values suggested by the microstructure and tracer release measurements (e.g., Ledwell et al. 1993). As shown above, the diapycnal buoyancy transfer in this parameter regime is dominated by the contribution from eddies.

To determine whether our analytical ($\epsilon \ll 1$) theory is adequate in the description of the numerical lens, we estimated the boundary layer width for the largest β run from the isotherm in Fig. 6. For consistency, the numerical width was computed as the nondimensional distance between the lens western edge and the point where the depth of this isotherm is maximal, resulting in

$$\delta_{\text{num}} = 0.20. \tag{31}$$

The analytical expression (25) yields, for $C = 0.04$ and $\beta = 1.12$,

$$\delta_{\text{theor}} = 5\frac{C}{\sqrt{\beta}} = 0.19. \tag{32}$$

Close agreement between the theoretical (32) and numerical (31) results once again confirms our interpretation of the boundary layer effects observed in the numerical simulations (Fig. 6).

5. Application to ocean gyres and circumpolar jets

Before addressing the geophysical applications of the foregoing model, it is important to realize that, because of its conceptual simplicity, this theory does not contain any ingredients that pertain specifically to the *unbounded* lens configuration. Thus, for example, the previously developed theory could be interpreted as pertaining to localized heating in a large basin in the presence of Ekman pumping or as a simple model of warmed, pumped flow confined by a circular vertical wall (but with upper-layer depth vanishing at the boundary). Because we demonstrated (section 4) that our shallow-water theory can account for the behavior of our numerical lens on an f plane and a β plane, we apply it to the more oceanographically relevant problems such as ocean gyres and circumpolar jets.

a. Gyres

Consider flow in a closed rectangular basin. The form of the wind stress is given, as before, by

$$w_e = -\cos(\pi y/L_y), \tag{33}$$

where L_y is the nondimensional meridional extent of the basin ($-0.5L_y < y < 0.5L_y$). Because here a purely geostrophic flow is considered, the condition of no flow across the boundary implies that the depth of the upper layer H_0 is constant along the perimeter of our domain. In trying to represent the ocean by one active layer, the choice of a suitable H_0 is always arbitrary. As a starting point, we consider the case of $H_0 = 0$, which enables us to retain a clear connection with the foregoing lens model. However, the theory can be trivially extended to a more general case with finite upper-layer thickness at the boundary.

The geostrophic shallow-water equations in which the eddies are parameterized using the scheme (8) were solved numerically subject to the boundary conditions of $h = 0$ at $x = 0$, 1 and $y = -L_y/2$, $L_y/2$. Parameters chosen for this calculation are representative of the subtropical gyres; the meridional extent of the basin is $L_y = 0.5$, roughly in accord with the aspect ratio of the North Atlantic subtropical gyre, and the nondimensional $\beta = 2$, so that the Coriolis parameter varies by 100% across the basin. The resulting steady state is shown in Fig. 11. It conforms well to our view of the subtropical gyre with a Sverdrup interior bounded on the west by a thin boundary layer controlled by our ''eddy-shedding'' mechanism.

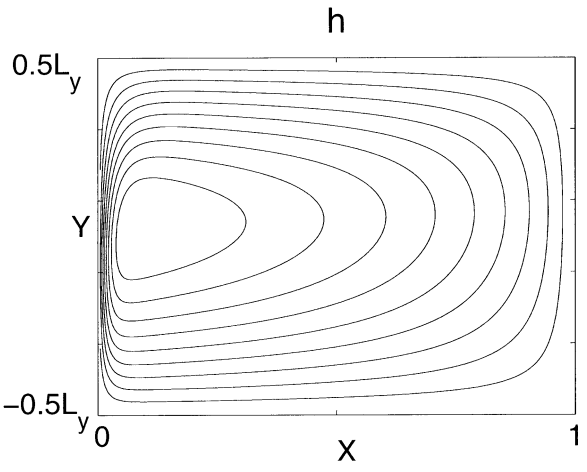

FIG. 11. Upper-layer depth for the steady state obtained by the numerical integration of (10) for $\beta = 2$, $L_y = 0.5$, and $C = 0.02$. Depth ranges from 0 to 0.9 nondimensional units.

To proceed analytically, we consider the governing equation [(10)] in the following two limits: $\epsilon \gg 1$ (the f-plane limit) and $\epsilon \ll 1$, where ϵ is given in (15).

1) OCEAN GYRES: $\epsilon \ll 1$

When eddy processes are weak in the interior and the β effect is strong ($\epsilon \ll 1$), a situation that we expect to be realized in ocean gyres, our solutions exhibit a boundary layer. The method of solving this asymptotic problem is very similar to that used above for the circular geometry (section 3), and will only be briefly outlined here. Following Stommel (1948) we separately consider the interior region $\epsilon \ll x < 1$ and a thin western boundary layer $0 < x < \epsilon$. The interior solution is obtained by setting C to zero in (10):

$$h_I = \sqrt{\frac{2f^2 w_e(1 - x)}{\beta}}, \tag{34}$$

and the boundary layer equations are obtained by stretching the zonal coordinate $x = \epsilon x_0$ near $x = 0$ and subsequently taking the $\epsilon \to 0$ limit:

$$\sqrt{\beta} h_B \frac{\partial h_B}{\partial x_0} + f^2 \frac{\partial^2}{\partial x_0^2} h_B = 0. \tag{35}$$

Integrating (35) twice in x_0 and applying the boundary conditions $h_B = 0$ at $x_0 = 0$ and $h_B = h_I(0, y)$ at $x_0 \to \infty$, we find

$$h_B = h_I(0, y) \tanh\left[\sqrt{\beta}\frac{x_0 h_I(0, y)}{2f^2}\right], \tag{36}$$

where $h_I(0, y)$ is given by (34).

When ϵ is small, the total volume of the upper-layer fluid, as well as the maximum depth of the thermocline,

$$h_{\text{dim}} \sim \sqrt{\frac{2LW_e f_{\text{dim}}^2}{g'\beta}}, \tag{37}$$

can be understood without invoking eddy processes. Thus, in contrast to the $\epsilon \gg 1$ limit, eddy dynamics is fundamental only in the vicinity of a western boundary current, where the intense eddy-shedding balances the total influx of buoyancy from the Ekman layer and determines the structure of the intensification region.

2) THE f-PLANE LIMIT: $\epsilon \gg 1$

In the f-plane limit, the governing equation (10) uniformly converges for, say, $L_y = 1$ to

$$\cos(\pi y) + C\nabla^2 h = 0. \tag{38}$$

Equation (38) has a simple analytical solution

$$h = \frac{\cos(\pi y)}{C\pi^2}\left\{1 - \cosh^{-1}\left(\frac{\pi}{2}\right)\cosh\left[\pi\left(x - \frac{1}{2}\right)\right]\right\}. \tag{39}$$

The maximum depth of the thermocline in this case occurs exactly at the center of the domain with value

$$h_{\max} = \frac{1}{C\pi^2}\left[1 - \cosh^{-1}\left(\frac{\pi}{2}\right)\right] \approx \frac{0.061}{C}. \tag{40}$$

In dimensional units, this corresponds to Marshall et al. (2002) scaling (1) for the depth of the heated and pumped f-plane lens with $c_h = 0.061/C$. For $C = 0.04$, this numerical factor is $c_h = 1.5$, which is of the same order as the Marshall et al. (2002) experimental estimate of 0.9; the discrepancy is most likely a consequence of the differing geometry and wind stress patterns employed. The volume of the upper-layer fluid and the whole structure of the lens is controlled entirely by eddy processes, just as in Marshall's laboratory experiments. It is interesting to note that the same depth scale appears in simple models of the Antarctic Circumpolar Current (ACC, e.g., Karsten et al. 2002) and in the theory considered below in section 5b.

b. Circumpolar jets

Having established that our simple model can give a consistent, although highly idealized, description of the zonally blocked flows, we now apply it to a geometry roughly corresponding to that of the southern ocean and its circumpolar flow. We assume a circularly symmetric mean flow and pump warm fluid down over the area bounded by the two concentric circles: $r_1 < r < r_2$, where $r = \sqrt{x^2 + y^2}$. Here we place the origin of the coordinate system at the pole and use the exterior radius of the flow as a unit of length, thereby setting $r_2 = 1$. In terms of our reduced-gravity model this geometric configuration translates to the requirement that the warm layer outcrops on the circle $r = r_1$ (see Fig. 12). For simplicity, we set $f = 1$ and $w_e = 1$ and assume that

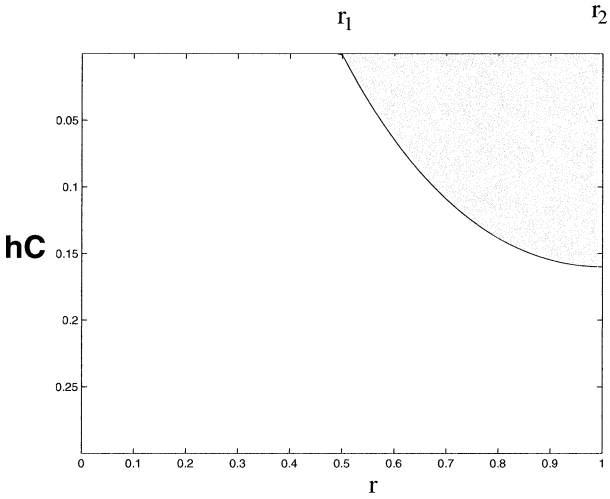

FIG. 12. Solution of the shallow-water equations for the ACC configuration in cylindrical coordinates (see the text). The shaded region represents the warm fluid in the active layer.

$\partial h/\partial r = 0$ at $r = r_1$, the equatorward extremity of our model.

For constant f the Sverdrup equation [(10)] degenerates into a statement of balance between the Ekman pumping and the cross-layer volume flux w^* (the $\epsilon \gg 1$ limit):

$$1 + C\nabla^2 h = 0, \qquad r_1 < r < r_2. \tag{41}$$

This is to be solved subject to the boundary conditions

$$h = 0 \qquad r = r_1$$

$$\frac{\partial h}{\partial r} = 0 \qquad r = 1. \tag{42}$$

Taking advantage of the circular symmetry of the flow field reduces (41) to an ordinary differential equation,

$$\frac{\partial^2 h}{\partial r^2} + \frac{1}{r}\frac{\partial h}{\partial r} = -\frac{1}{C}, \tag{43}$$

whose general solution is given by

$$h = A + B\log(r) - \frac{1}{4C}r^2. \tag{44}$$

The coefficients A and B are determined from the boundary conditions (42)—they are $A = -(2\log r_1 - r_1^2)/4C$ and $B = 1/(2C)$. The resulting solution is plotted in Fig. 12 for $r_1 = 0.5$. Despite its highly idealized nature, it captures the basic structure and the zero-order dynamics of the prototype ACC solutions discussed in Karsten et al. (2002). Particularly suggestive is the similarity of the radial distribution of buoyancy in Fig. 12 and in the corresponding Fig. 6a in Karsten et al. (2002).

The depth scale of our solution is still given by (1). To be specific, let us estimate the maximum depth for the solution in Fig. 12. The largest value of depth $h_{\max} = 0.16/C$ in Fig. 12 implies that, for $C = 0.04$, the maximum dimensional depth is

$$h_{\text{dim}} = 4\sqrt{\frac{f_0 W_e}{g'}}L. \tag{45}$$

For the typical parameter values for the ACC (used by Karsten et al. 2002), namely, $W_e = 8 \times 10^{-7}$ m s^{-1}, $L = 2000$ km, $g' = 5 \times 10^{-3}$ m s^{-2}, $f_0 = 1.2 \times 10^{-4}$ s^{-1}, the depth scale from (45) is about $h_{\text{dim}} = 1.1$ km, in broad accord with the observations discussed in Karsten and Marshall (2002).

6. Discussion and conclusions

We have discussed the evolution of a buoyant lens, heated and pumped from the surface on a β plane. An important qualitative question is whether the structure and dynamics of such a flow are controlled by laminar adiabatic processes, as assumed in ideal thermocline theories, or by turbulent transfer by baroclinic eddies that are fundamental to the equilibration of the f-plane lens studied in Marshall et al. (2002).

Numerical eddy-resolving simulations show that equilibration of the β-plane lens has aspects in common with that on the f plane (Marshall et al. 2002). In both cases the volume of warm water gained at the surface from the Ekman pumping is balanced by the volume loss due to eddy shedding. However, the β-plane lens is not circularly symmetric but is tilted to the west (Fig. 6), and the eddy activity is mostly limited to the western part, in response to the westward intensification of a mean flow. When β is systematically increased, the circulation becomes increasingly asymmetric, and, for the largest values of β employed, the lens transforms into a structure that can be described as a quasi-laminar Sverdrupian gyre bounded on the west by a thin boundary layer. The ''leaky'' boundary layer is markedly different from more conventional models of western intensification. It provides the means by which the lens (adiabatic over most of its area) can balance the influx of warm water from the Ekman layer. Formation and detachment of eddies tend to increase the mean PV by squeezing vortex columns, a process that makes possible to close the circulation problem even in the absence of any momentum diffusion.

Diagnostics of our numerical lenses show that

1) the flux of warm water from the Ekman layer is, to leading order, balanced by the cross-isopycnal eddy transfer as implied in (11);
2) the intensity of the eddy transfer is greatly enhanced in the vicinity of the swift and energetic currents; and
3) the structure and dynamics of the equilibrated lens reflect a balance between the effects of Ekman pumping and squeezing of the Taylor columns by the volume release by eddies [see (12)].

In section 3, we constructed a simple theoretical model of the phenomenon using a heuristic parameterization of eddies, and we demonstrated (section 4) that the key properties of the numerical solutions are consistent with the analytical results. If β is sufficiently large (the $\epsilon \ll 1$ limit), laminar Sverdrup dynamics determines such important characteristics as the maximum depth of the lens, but the eddy shedding is shown to be essential for balancing the vorticity and volume budgets and must be included in a complete description of the oceanic thermocline. In the limit $\epsilon \gg 1$, however, eddy shedding controls the depth and volume of the lens and leads us to a model that captures, we believe, the essential dynamics of circumpolar jets, albeit in an abstract manner. Thus, the single idealized framework explored here is able to represent gyre dynamics (small ϵ) and circumpolar jets (large ϵ). Solutions obtained using the thickness-diffusion parameterization (section 3) and a lateral-flux closure (appendix) are qualitatively similar, suggesting that our theoretical results are not sensitive to a specific eddy closure. In section 5, we applied our ideas, initially developed for the lens problem, to construct a simple model of subtropical gyres and circumpolar jets.

Analysis of our idealized solutions suggests that eddy transfer may be a central mechanism in the maintenance of the large-scale stratification of the thermocline. Note, however, that the only way in which the lens can reach a steady state is by eddy flux, at least when the vertical mixing is small. How, then, might these results pertain to the real ocean?

Possible application to the North Atlantic subtropical gyre

The importance of eddies for ACC dynamics seems to be generally accepted (e.g., McWilliams et al. 1978; Marshall 1981; Johnson and Bryden 1989; Karsten et al. 2002), but the role of eddies in the gyre dynamics is much less clear. Could a volume balance between Ekman pumping and eddy shedding be at work, say, in the North Atlantic subtropical gyre?

The abundance of eddies in the North Atlantic and their ability to transport fluid over thousands of kilometers is well established (Olson 1991). The largest and most energetic eddies in the North Atlantic are Gulf Stream rings, reaching up to 140 km in diameter and extending to depths of about 750 m. A warm-core ring of this size effectively transports, according to the estimate of a ''trapped zone'' (e.g., Flierl 1981; Angel et al. 1983) in excess of 3×10^{13} m^3 of fluid away from the subtropical gyre. The exact value for the net eddy transport of subtropical thermocline water is uncertain, because some of the rings, weakened and partially dispersed, are subsequently reabsorbed by the Gulf Stream. However, it is plausible that the observed shedding of five–eight eddies per year results in a volume flux comparable to the net input of a warm water from the Ekman layer over the area of subtropical gyre (about 8 Sv $\approx 24 \times 10^{13}$ m^3 yr^{-1}). In addition to such dramatic events as the shedding of the Gulf Stream rings, the observed smaller and less-coherent mesoscale and submesoscale eddies may also contribute to this balance.[1]

Thus, order-of-magnitude estimates are not in conflict with the key assumptions of our theory for gyres. Although closing the real oceanic circulation undoubtedly involves a number of competing diabatic processes, the eddy-shedding mechanism explored here may be a key player. Further progress is anticipated from the analysis of eddy-shedding effects in a more general framework, such as more realistic geometry and forcing as well as inclusion of other processes known to influence the dynamics of the western boundary layers. Such calculations are in progress and will be reported later.

Acknowledgments. We thank the Physical Oceanography Division of the National Science Foundation, whose support made this study possible. Geoffrey Vallis and an anonymous referee gave us very useful comments.

APPENDIX

Lateral-Flux Closure

Although the solutions obtained using the thickness-diffusion closure (section 3) are internally consistent, it is desirable to examine to what extent the results depend on the choice of a particular eddy parameterization scheme. The closure scheme for eddies that will be considered in this appendix is based on a physical picture (qualitatively supported by the numerical experiments described in section 2) in which eddies move laterally away from the lens, transporting the trapped fluid across the density front. We express this process thus:

$$w^*_{\text{dim}} = U_{\text{eddy}} |\nabla h_{\text{dim}}|, \tag{A1}$$

where U_{eddy} is the eddy-induced horizontal warm-water flux velocity (see the schematic in Fig. 1). If we assume that this flux depends on the *local* large-scale velocity—$U_{\text{eddy}} = C_1 |\boldsymbol{v}|$—then the resulting nonlinear closure scheme is, nondimensionally,

$$w^* = \frac{C_1}{f} |\nabla h|^2, \tag{A2}$$

where the constant C_1 is a measure of the efficiency of eddy shedding. It plays a role analogous to that C played in the thickness-diffusion closure.

As before (section 3), we integrate (5) numerically but now with w^* given by (A2). A finite-difference code was used in which a small Laplacian friction (of order

[1] It should be mentioned that other mechanisms have been suggested to explain the volume balance in the subtropics. These include, for example, the baroclinic cross-gyre exchange flows as in Chen and Dewar (1993).

$\sim 10^{-3}$) was added to (5) to control numerical stability. This integration yielded a steady solution (not shown) very similar to the one in Fig. 7 as the steady state again consisted of a Sverdrup-type interior connected to a thin western boundary layer.

An appealing feature of the ''lateral-flux'' closure (A2) is that it offers considerable analytical advantages, making it possible to obtain explicit solutions that are valid regardless of the value of C_1. The following analysis is based on the observation that our solutions (see Figs. 7, 11) are approximately symmetric about the central latitude ($y = 0$), even for substantial values of β. Such a symmetry is a consequence of the absence of inertial terms in the momentum equations [(5)] and the symmetry of the Ekman pumping field (w_e), which render the governing equations [(5)] symmetric. For a symmetric h field,

$$\left.\frac{\partial h}{\partial y}\right|_{y=0} = 0, \tag{A3}$$

and then (7) at $y = 0$ reduces to an ordinary differential equation,

$$\frac{\beta}{f}\frac{\partial h}{\partial x}h = f\left(-1 + C_1 v \frac{\partial h}{\partial x}\right). \tag{A4}$$

When h is rescaled using $\hat{h}(x) = \sqrt{\beta}h(x, ½)$, the equation for the thermocline depth along the central latitude reduces to

$$\frac{\partial \hat{h}}{\partial x}\hat{h} = -1 + \sigma\left(\frac{\partial \hat{h}}{\partial x}\right)^2. \tag{A5}$$

Note that here the governing parameter is $\sigma = C_1/\beta$, different from that used previously (section 3).

The *first*-order differential equation (A5) must be solved subject to the *two* boundary conditions: $\hat{h}(0) = 0$ and $\hat{h}(1) = 0$. This, generally, overdetermines the problem, indicating that discontinuities in $\partial\hat{h}/\partial x$ may occur. It is well known that such discontinuities arise as a consequence of using simplified equations in which (small) terms involving higher-order derivatives are neglected. We invoke the principle of minimizing the number of discontinuities and look for a solution of (A5), which has no more than one discontinuity of the slope.

Solving (A5) for $\partial\hat{h}/\partial x$ as a function of h yields two branches:

$$\frac{\partial \hat{h}}{\partial x} = -\frac{2}{\hat{h} + \sqrt{\hat{h}^2 + 4\sigma}} \quad \text{and} \tag{A6}$$

$$\frac{\partial \hat{h}}{\partial x} = \frac{1}{2\sigma}\left(\hat{h} + \sqrt{\hat{h}^2 + 4\sigma}\right). \tag{A7}$$

Because the solution of (A6) is a decreasing function of x, and (A7) gives an increasing $\hat{h}(x)$, there is only one physically meaningful solution that has (at most) one slope discontinuity. Such a solution can be constructed by integrating (A7) from $x = 0$ to the point of maximum depth δ (to be determined below), and using (A6) for the interval $\delta < x < 1$.

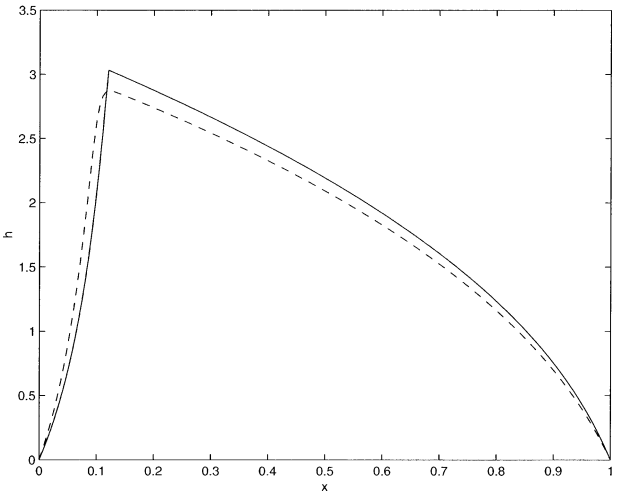

FIG. A1. Comparison of the analytical solution for the depth at the center of the domain with the result of numerical integration. Theoretical expression is presented by solid line; dashed line is the iterative solution.

Equations (A6) and (A7) were reduced to the known integrals (Abramovitz and Stegun 1964) and solved exactly. The resulting solution, which satisfies the boundary conditions at $x = 0$ and $x = 1$, is

$$x = \frac{\hat{h}}{2}\sqrt{\left(\frac{\hat{h}}{2}\right)^2 + \sigma} - \frac{\hat{h}^2}{4} + \sigma \ln\left[\frac{\hat{h}}{2\sqrt{\sigma}} + \sqrt{\left(\frac{\hat{h}}{2\sqrt{\sigma}}\right)^2 + 1}\right], \quad 0 < x < \delta, \quad \text{and} \tag{A8}$$

$$1 - x = \frac{\hat{h}}{2}\sqrt{\left(\frac{\hat{h}}{2}\right)^2 + \sigma} + \frac{\hat{h}^2}{4} + \sigma \ln\left[\frac{\hat{h}}{2\sqrt{\sigma}} + \sqrt{\left(\frac{\hat{h}}{2\sqrt{\sigma}}\right)^2 + 1}\right], \quad \delta < x < 1. \tag{A9}$$

The cross-over point δ is determined by matching $\hat{h}$ from the eastern part of the basin (A9) with that from the western solution (A8).

Figure A1 is a comparison of our analytical solution (A8) and (A9) for $\sigma = 0.055$ with the corresponding numerical iterative solution of (5). Agreement between the analytical and numerical results is remarkable, especially in view of the fact that a (weak) interfacial drag was added to (5) for numerical integration. These frictional terms increase the order of equations and make our boundary value problem well-posed, whereas the

choice of a suitable analytical solution did involve some heuristic arguments.

Although the expressions in (A8) and (A9) are valid for all values of σ, it is illuminating to consider the two asymptotic limits in detail: $\sigma \to \infty$ and $\sigma \to 0$. In the $\sigma \to 0$ limit, the eastern part of the solution (A9) uniformly converges to the Sverdrup form

$$\hat{h} = \sqrt{2(1 - x)}. \tag{A10}$$

whereas the western solution (A8) has a steep (singular) slope at $x = 0$ [$(\partial\hat{h}/\partial x)|_{x=0} = 1/\sqrt{\sigma}$] indicating that the western part reduces to a thin boundary layer. Details of the asymptotic structure of the boundary layer could be easily deduced by examining (A8) and matching the depth with that from (A10). Thus, for (say) boundary layer width, we obtain

$$\delta \sim \frac{\sigma}{2} \ln\left(\frac{1}{\sigma}\right). \tag{A11}$$

The maximum depth of the thermocline occurs at $x = \delta$ and its dimensional scaling for $\sigma \to 0$ is

$$h_{\text{dim}} \sim \sqrt{\frac{2LW_e f_{\text{dim}}^2}{g'\beta}}, \tag{A12}$$

a well-known expression that can be derived directly from the Sverdrup relationship for the ideal one-and-one-half-layer fluid (Pedlosky 1996).

Now consider the opposite limit $\sigma \to \infty$. This is a situation realized, for example, in the Marshall et al. (2002) laboratory f-plane experiments. In this case (A8) and (A9) reduce to

$$\hat{h} = \frac{1}{\sqrt{\sigma}} x, \qquad 0 < x < \frac{1}{2}, \tag{A13}$$

$$\hat{h} = \frac{1}{\sqrt{\sigma}}(1 - x), \qquad \frac{1}{2} < x < 1, \tag{A14}$$

and $\delta \to$ ½. The maximum depth of the thermocline is then $\hat{h} = 1/(2\sqrt{\sigma})$. In dimensional units this reduces to (1), which is Marshall et al.'s scale for the depth of the heated and pumped f-plane lens.

Thus, just as obtained with the closure equation in (8), for sufficiently large β, the solution consists of a quasi-adiabatic interior, whose depth scale can be determined from ideal thermocline theory, and a narrow western boundary layer where eddy transfer is essential. When β is small, eddy shedding is distributed uniformly throughout the lens area, and the depth scale is set by eddies. Regardless of which parameterization of eddy transfer is adopted, the expression for the maximum depth is consistent with (1). However, some details of the solution are closure dependent. For example, we observed that the scaling of the boundary layer width in the large-β case is close to $O(1/\beta)$ for the lateral-flux closure considered in this appendix, whereas the thickness-diffusion parameterization implies $\delta \propto 1/\sqrt{\beta}$. It is yet to be determined which scaling provides a superior description of the eddying β-plane lens.

REFERENCES

Abramovitz, M., and I. A. Stegun, 1964: Handbook of mathematical functions. *Appl. Math. Ser.,* **55,** 1046 pp.

Angel, M. V., and M. J. R. Fasham, 1983: Eddies and biological processes. *Eddies in Marine Science*, Springer-Verlag, 492–524.

Chen, L. G., and W. K. Dewar, 1993: Intergyre communication in a three-layer model. *J. Phys. Oceanogr.,* **23,** 855–878.

Flierl, G. R., 1981: Particle motions in large amplitude wave fields. *Geophys. Astrophys. Fluid Dyn.,* **18,** 39–74.

Gent, P. R., and J. C. McWilliams, 1990: Isopycnal mixing in ocean circulation models. *J. Phys. Oceanogr.,* **20,** 150–155.

Johnson, G. C., and H. L. Bryden, 1989: On the size of the Antarctic Circumpolar Current. *Deep-Sea Res.,* **36,** 39–53.

Jones, H., and J. Marshall, 1997: Restratification after deep convection. *J. Phys. Oceanogr.,* **27,** 2276–2287.

Karsten, R., and J. Marshall, 2002: Testing theories of the vertical stratification of the ACC against observations. *Dyn. Atmos. Oceans,* **36,** 233–246.

——, H. Jones, J. Marshall, and R. M. Wardle, 2002: On eddy transport and the stratification of the Circumpolar Current. *J. Phys. Oceanogr.,* **32,** 39–54.

Ledwell, J., A. Watson, and C. Law, 1993: Evidence for slow mixing across the pycnocline from an open-ocean tracer-release experiment. *Nature,* **367,** 701–703.

Luyten, J., J. Pedlosky, and H. Stommel, 1983: The ventilated thermocline. *J. Phys. Oceanogr.,* **13,** 292–309.

Marshall, J., 1981: On the parameterization of geostrophic eddies in the ocean. *J. Phys. Oceanogr.,* **11,** 257–271.

——, A. Adcroft, C. Hill, L. Perelman, and C. Heisey, 1997a: A finite-volume, incompressible Navier Stokes model for studies of the ocean on parallel computers. *J. Geophys. Res.,* **102** (C3), 5753–5766.

——, C. Hill, L. Perelman, and A. Adcroft, 1997b: Hydrostatic, quasi-hydrostatic, and nonhydrostatic ocean modeling. *J. Geophys. Res.,* **102** (C3), 5733–5752.

——, H. Jones, R. Karsten, and R. Wardle, 2002: Can eddies set ocean stratification? *J. Phys. Oceanogr.,* **32,** 26–38.

McWilliams, J. C., W. R. Holland, and J. S. Chow, 1978: A description of numerical Antarctic Circumpolar Currents. *Dyn. Atmos. Oceans,* **2,** 213–291.

Olson, D. B., 1991: Rings in the ocean. *Ann. Rev. Earth Planet. Sci.,* **19,** 283–311.

Pedlosky, J., 1996: *Ocean Circulation Theory.* Springer-Verlag, 488 pp.

——, and H. P. Greenspan, 1967: A simple laboratory model for the ocean circulation. *J. Fluid Mech.,* **27,** 291–304.

Robinson, A. R., and H. Stommel, 1959: The oceanic thermocline and the associated thermohaline circulation. *Tellus,* **11,** 295–308.

Samelson, R. M., and G. K. Vallis, 1997: Large-scale circulation with small diapycnal diffusion: The two-thermocline limit. *J. Mar. Res.,* **55,** 223–275.

Stewart, R. W., 1964: The influence of friction on inertial models of oceanic circulation. *Studies on Oceanography,* Tokyo University, 3–9.

Stommel, H., 1948: The westward intensification of wind-driven ocean currents. *Trans. Amer. Geophys. Union,* **29,** 202–206.

Vallis, G. K., 2000: Thermocline Theories and WOCE: A Mutual Challenge. *International WOCE Newsletter,* No. 39, WOCE International Project Office, Southampton, United Kingdom, 30–33.

Visbeck, M., J. Marshall, T. Haine, and M. Spall, 1997: Specification of eddy transfer coefficients in coarse-resolution ocean circulation models. *J. Phys. Oceanogr.,* **27,** 381–402.